# Arbitrary orientation of atoms and molecules via coherent population trapping by elliptically polarized light

Valery Milner, Boris M. Chernobrod, and Yehiam Prior
*Chemical Physics Department, Weizmann Institute of Science, Rehovot 76100, Israel*
(Received 8 April 1998; revised manuscript received 1 February 1999)

The interaction of laser light of arbitrary polarization with systems of high angular momentum is considered. We show that elliptically polarized light creates an anisotropic spatial distribution of atomic and molecular angular momentum which is qualitatively different from the alignment and orientation induced by light of circular or linear polarization. Multilevel coherent population trapping within a manifold of ground-state magnetic sublevels results in a nonclassical behavior of a high-$J$ molecular rotor. The classical approximation for the angular momentum distribution is compared with the exact quantum calculations, and is shown to fail in cases of long interaction times and high intensities of the exciting light. In these limits, the quantum uncertainty defines the spatial width of the angular distribution. The applicability of the classical treatment is analyzed and found to be different in the cases of $J \rightarrow J-1$ and $J \rightarrow J$ transitions. A biaxial spatial orientation with two preferential axes of rotation is experimentally created in sodium atoms via coherent population trapping by elliptically polarized light. A method for producing an arbitrary orientation of atomic angular momentum by magnetic field assisted coherent population trapping is proposed. [S1050-2947(99)01708-4]

PACS number(s): 33.80.Ps, 42.50.Gy, 33.20.Sn

## I. INTRODUCTION

In 1950, Kastler [1] proposed optical pumping (OP) as a method of producing anisotropic angular momentum distribution in the electronic ground state of atoms through the resonant absorption of circularly polarized light followed by spontaneous emission. Optical pumping within an energy level which is degenerate over its magnetic sublevels can be viewed as originating from the existence of sublevels which are uncoupled from the exciting light. The population of such (one or more) uncoupled sublevels may grow if there is spontaneous emission back to the same ground state (closed system), or remain unperturbed while all other sublevels are excited by the light and decay to other levels (open system). In both cases, the result of the repeated absorption-emission cycles of the OP process is a nonequilibrium population distribution of the degenerate magnetic sublevels. In quantum terminology, a nonuniform population of magnetic sublevels means a spatial anisotropy of the angular momentum. The uncoupled magnetic sublevels (or $m$ sublevels where $m$ is the projection of the total angular momentum $J$) are defined by the type of transition and the polarization of the exciting light. As an example, circularly polarized ($\sigma$) light interacting with a $P$ type molecular transition ($J \rightarrow J-1$) does not couple the sublevels $m=J, J-1$ to the excited state, while for the $Q$ transition ($J \rightarrow J$), it is $m=J$ which is not coupled [see Figs. 1(a) and 1(b)]. In both cases the OP causes *orientation* (axial and directional spatial distribution) of the ground state along the wave vector $\mathbf{k}$ of the exciting light. *Alignment* (axial but nondirectional spatial distribution) of the level may be created by linearly polarized ($\pi$) excitation which (depending on the transition) does not deplete the sublevels $m=\pm J$ (longitudinal alignment) or $m=0$ (transverse alignment).

The redistribution of the ground-state angular momentum due to optical pumping by polarized light has been thoroughly studied by Ducloy [2–4], Zare [5,6], Auzin'sh and Ferber [7], and Bergmann [8]. In recent years, several experimental groups have demonstarted many important related effects such as polarization rotation [9,10], spatial splitting [11], and spatial deflection [12] of laser beams propagating in an optically oriented medium.

As a rule, a *uniaxial* (or cylindrical) symmetry of the ground-state angular momentum distribution was considered

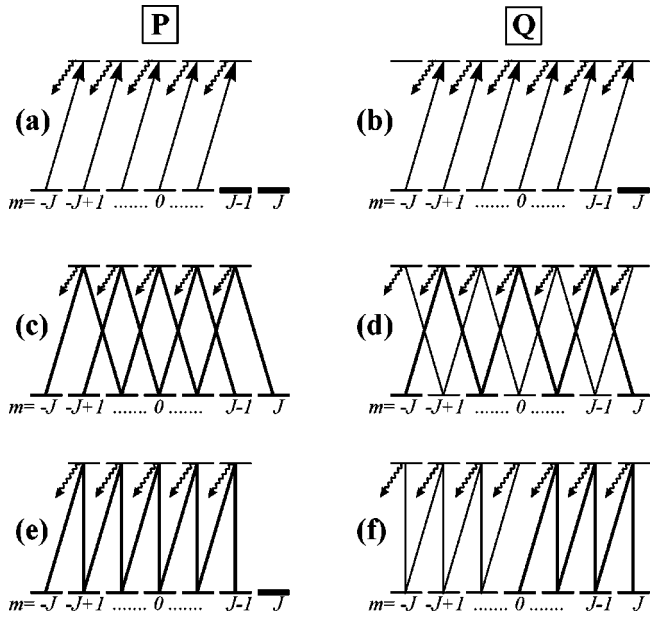


FIG. 1. Coupling schemes between the $m$ sublevels within $P$ (left column) and $Q$ (right column) transition. The quantization axis is taken to be directed along the light propagation (a)–(d) for circular (a),(b) and elliptical (c),(d) polarization, and along the EDS axis (e) and (f). Sublevels participating in the coherent population trapping are plotted by thick lines, and the noncoupled sublevels are depicted by bold.

 

by most authors. A single symmetry axis exists in the cases of $\sigma$ or $\pi$ excitation, and it is collinear with the light propagation direction or the polarization vector, respectively. For these polarizations, if the appropriate quantization axis is chosen, the multilevel system may be decomposed into a set of independent two-level subsystems and one (or more) noncoupled sublevel(s) [Figs. 1(a) and 1(b)]. Thus, the steady state density matrix remains diagonal, and the orientation (alignment) of the ensemble is fully defined by the population of the magnetic sublevels without any cross coherence terms. However, such a convenient choice of the quantization axis is not possible for the general case of arbitrary (*elliptical*) polarization of the exciting light, when the cross coherence terms cannot be avoided in *any* quantization basis [Figs. 1(c) and 1(d)]. Several theoretical papers [7,13,14] analyzed the quantum interaction of a multilevel system with elliptically polarized light, but the geometrical picture of the angular momentum distribution and its experimental ramifications have not been appreciated.

In this article we apply an optical pumping approach onto the general case of elliptical polarization, and show, both theoretically and experimentally, that the result is a very unique *biaxial* spatial distribution of angular momentum. Moreover, by applying a weak magnetic field, this distribution is transformed into a uniaxial orientation in which the symmetry axis depends on the polarization ellipticity, and may be changed without changing the exciting light propagation direction. Consequently, our method can produce an *arbitrary orientation* of a molecular (atomic) ensemble by a single laser beam and a properly oriented magnetic field.

Whereas $\sigma$ ($\pi$) light optically pumps the system into a single, or at most two, uncoupled $m$ sublevel, optical pumping by elliptically polarized light, as we have shown recently [15], transfers the population into a multilevel elliptical dark state (EDS)—a coherent superposition of many magnetic sublevels which is completely uncoupled from the exciting light. The analysis of the angular momentum distribution of the elliptical dark state requires a full quantum treatement of the interaction, which is presented in Sec. II. For high-$J$ transitions, one might expect to treat a molecule as a classical rotor characterized by the spherical coordinates of its angular momentum $J$. The classical approach is considered in Sec. III, where we show that even though coherences are neglected, the spatial distribution of $J$ may nevertheless be estimated and observed. In Sec. IV we analyze the nonclassical aspects of the resonant interaction of a molecular rotor with a large angular momentum, and give the limits of applicability and the drawbacks of the classical analysis. Finally, in Sec. V, the method of observation and the experimental proof of biaxial spatial orientation are presented. The possiblity of creating arbitrary orientation of atoms and molecules, and the potential utilization of the elliptical dark states for optical magnetometry are discussed in Sec. VI.

## II. QUANTUM APPROACH

Consider a model system of two levels with energies and angular momenta $E'',J''$ and $E',J'$ for the ground and excited states, respectively, degenerate over the projection of angular momentum (Fig. 1). The interaction of this system with resonant electromagnetic field of polarization $\mathbf{q}$, $\mathbf{E}(t)=\mathcal{E}\mathbf{q}e^{-i\omega t}+\text{c.c.}$, is described by the nonstationary Schrödinger equation

$$i\hbar\frac{\partial}{\partial t}\Psi(t)=[\hat{H}_0+\hat{V}(t)]\Psi(t), \tag{1}$$

with the interaction Hamiltonian $\hat{V}(t)=-\mathbf{E}(t)\mathbf{d}$, where $\mathbf{d}$ is the transition dipole moment between the $J''$ and $J'$ states. In the interaction picture, the solution is sought in the form

$$\Psi(t)=e^{-i(E'/\hbar)t}\sum_{|m|\leqslant J'}a_m(t)\psi'_m+e^{-i(E''/\hbar)t}\sum_{|m|\leqslant J''}b_m(t)\psi''_m, \tag{2}$$

where the amplitudes $a_m(t)$ correspond to the excited state levels, the amplitudes $b_m(t)$ correspond to the ground-state levels, and $\psi_m$ is the eigenfunction of the unperturbed Hamiltonian $\hat{H}_0$ corresponding to the magnetic sublevel with the quantum number $m$. In the rotating-wave approximation, Eq. (1) reduces to a set of coupled differential equations [16]:

$$\begin{aligned} i\hbar\dot{a}_m(t)&=V_{m,m-1}b_{m-1}(t)+V_{m,m+1}b_{m+1}(t)-\gamma a_m(t),\\ i\hbar\dot{b}_m(t)&=(V_{m-1,m})^*a_{m-1}(t)+(V_{m+1,m})^*a_{m+1}(t), \end{aligned} \tag{3}$$

where the index $m$ covers all possible magnetic quantum numbers for each level and $2\gamma$ is added as the spontaneous emission decay rate of the excited state population (assumed equal for all sublevels). Here we assume that spontaneous emission is the only relaxation channel of the system under investigation, and consider an *open transition*, where a spontaneously emitted photon does not bring a system back to its initial ground state. This assumption is very well justified for molecular systems.

The matrix elements of the interaction Hamiltonian may be written according to the Wigner-Eckart theorem as a product of dynamic and angular parts:

$$V_{m,m'}=\mathcal{E}d\times\left[q_{\Delta m}\cdot(-1)^{J''-m}\cdot\begin{pmatrix} J'' & 1 & J'\\ -m & \Delta m & m'\end{pmatrix}\right], \tag{4}$$

where the reduced matrix element $d=\langle J''||\mathbf{d}||J'\rangle$ is independent on the magnetic quantum numbers, $\Delta m=m-m'$, and $q_{0,\pm1}$ are the components of the polarization vector in cyclic coordinates.

### A. Coherent population trapping by elliptically polarized light

If the quantization axis is chosen along the propagation direction of the light, then the components of the polarization vector are

$$q_{+1}=-e^{-i\delta}\cos\left(\varepsilon-\frac{\pi}{4}\right),\quad q_0=0,\quad q_{-1}=e^{i\delta}\cos\left(\varepsilon+\frac{\pi}{4}\right). \tag{5}$$

Here the parameter $\delta$ ($0\leqslant\delta\leqslant\pi$) determines the orientation angle of the polarization ellipse (the angle between its major axis and the coordinate axis $\mathbf{x}$), and $\tan(\varepsilon)$ ($-\pi/4\leqslant\varepsilon\leqslant\pi/4$) is the ratio between the minor and major axes of the polarization ellipse.

In the case of linearly or circularly polarized radiation, the degenerate multilevel system decomposes into a set of independent two-level subsystems and noncoupled sublevels, and it is possible to find analytical solutions of Eq. (3). The ''edge'' sublevels with the projection $m=\pm J$ or $m=J,J-1$ $(-J,-J+1)$, depending on the type of transition and light polarization, are noncoupled and remain populated [see, for example, Figs. 1(a) and 1b)]. All other sublevels are emptied out with the characteristic rate $\gamma_{\mathrm{op}}$ of the optical pumping, which is the lower rate between the spontaneous emission and laser excitation rates

$$\gamma_{\mathrm{op}} \approx \begin{cases} \gamma & \text{for} \quad \varkappa \gg 1, \\ \varkappa\gamma & \text{for} \quad \varkappa \ll 1, \end{cases} \tag{6}$$

where $\varkappa$ is the saturation parameter,

$$\varkappa = \frac{1}{2J+1}\frac{(\mathcal{E}d)^2}{(2\hbar\gamma)^2}$$

(the degeneracy factor is included as in Ref. [17]). Note, that in the case of a closed (or partially closed) transition, the optical pumping rate is decreased due to the possible spontaneous emission back to the same $m$ sublevel. Nevertheless, $\gamma_{\mathrm{op}}^{-1}$ $(t_{\mathrm{op}})$ determines the relevant time scale of the OP, which we will use in the present analysis.

When the radiation has an arbitrary (elliptical) polarization, the situation is not as simple. *All* the ground state magnetic sublevels are coupled to the excited state [Figs. 1(c) and 1(d)], and therefore an open system may be naively expected to be emptied in a few excited state lifetimes. However, for $P(J)$ $(J\rightarrow J-1)$ and $Q(J)$ $(J\rightarrow J)$ transitions, a noncoupled state $\Psi_{\mathrm{NC}}$ satisfying

$$\hat{V}(t)\Psi_{\mathrm{NC}} \equiv 0, \tag{7}$$

may still be found, as was theoretically shown in Refs. [13,14,16]. Unlike the case of linear and circular polarization, $\Psi_{\mathrm{NC}}$ is a coherent superposition of *many* ground $m$ sublevels. Nevertheless, the optical pumping mechanism remains the same: after several characteristic times $t_{\mathrm{op}}$, the system is optically pumped into the steady state $\Psi_{\mathrm{NC}}$ and stops absorbing or rescattering the exciting light, being in a so-called *dark state*.

In general, it is very difficult to find an exact analytical time-dependent solution of Eq. (3). To illustrate the temporal behavior of a multilevel system driven by elliptically polarized light, a numerical solution of Eq. (3) for the $P(10)$ transition is presented in Fig. 2. (A complete description of the numerical procedure and analysis of different types of transitions is given in our earlier paper [18].) The important result shown in Fig. 2(a) is the long time steady state population which is achieved after the transient Rabi oscillations decay. The absence of Rabi oscillations at the end of the process means that there is no further interaction with the exciting light, even though the ground-state population is nonzero. On the other hand, the excited-state sublevels (gray lines) are not populated, attesting to the fact that this is not a saturation phenomenon, but rather a coherent population trapping (CPT). CPT was originally demonstrated and is generally discussed for a three-level $\Lambda$ system [19,20]. The

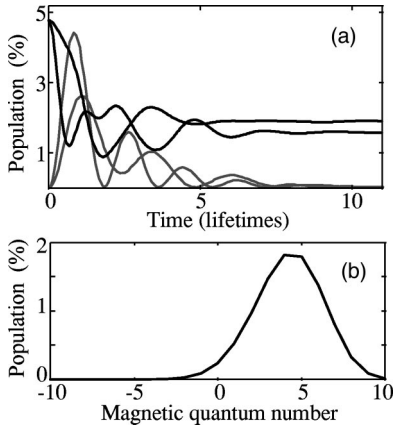


FIG. 2. (a) Population dynamics of several ground state magnetic sublevels of a $P(10)$ transition excited by elliptically polarized light ($\varepsilon=0.4$). The stationary ground state (bold line) nonzero population after 10 lifetimes represents the multilevel coherent population trapping. The excited state population is depicted by gray lines. (b) The population distribution among magnetic sublevels in the elliptical dark state created within a $P(10)$ transition.

effect stems from the destructive interference of the quantum interaction amplitudes, and was generalized by us to the multi-$\Lambda$ configuration [18]. Note, that transitions $R(J)$ $(J\rightarrow J+1$, not shown in Fig. 1) do not contain a $\Lambda$-type coupling, and therefore do not support CPT [a noncoupled state cannot be constructed to satisfy the condition of Eq. (7)].

Coherent population trapping is an important (though not necessary) condition for the optical orientation of open systems. To show this, consider the properties of a dark state prepared by elliptically polarized light [or elliptical dark state (EDS)]. As we have recently demonstrated in Ref. [21], the character of the EDS is completely determined by the polarization of the exciting light. Namely, the $m$-sublevel population distribution of the EDS [Fig. 2(b)] and the cross coherences between them reflect the light ellipticity: the eccentricity and the orientation of the polarization ellipse. The population distribution is very different for different transition types. Consider the $J\rightarrow J$ transition excited by light of elliptical polarization with $|q_{+1}|>|q_{-1}|$ [Fig. 1(d)]. The rightmost $\Lambda$ in the multi-$\Lambda$ chain consists of the two ground-state sublevels $m=J-2,J$ and $m=J-1$ of the excited state. For these sublevels we always have $|V_{J-1,J-2}|>|V_{J-1,J}|$, since the $3j$ symbol in Eq. (4) is larger for the smaller $|m'|$. The stationary condition for these $m$ sublevels is [Eq. (3)]:

$$a_{J-1}=0, \quad V_{J-1,J-2}b_{J-2}+V_{J-1,J}b_J=0, \tag{8}$$

whence the ''edge'' sublevel $(m=J)$ in the ground-state manifold is always more populated: $|b_J|^2>|b_{J-2}|^2$. However, for the $J\rightarrow J\pm 1$ transitions, the $3j$ symbol has a maximum at $|m'|=J$, and the last inequality is not necessarily true. In contrast, here the most populated sublevel is determined by the balance between the light ellipticity and the $m$ dependence of the corresponding $3j$ symbol. This point is illustrated in Fig. 2(b), where the maximum of the population distribution clearly corresponds to an intermediate $m$ number.

### B. Choice of the quantization axis

Before looking at the spatial distribution of angular momentum of the elliptical dark state, it is instructive to support the analysis by a different approach, first presented in Ref. [22]. Consider a new quantization axis $n(\theta,\delta)$, which in the old basis is specified by two spherical angles: an arbitrary angle $\theta$ and the orientation angle of the polarization ellipse $\delta$ (Fig. 3). To find the polarization vector $\mathbf{q}'$ in the new coordinate system, one has to perform the rotation of $\mathbf{q}$ by angle $\theta$ around $\mathbf{y}$ axis and then by $\delta$ around $\mathbf{z}$ axis (also equivalent to the rotation by angle $\theta$ around the minor axis of the polarization ellipse): $\mathbf{q}'=\hat{U}(\theta,\delta)\cdot\mathbf{q}$. The rotation matrix $\hat{U}(\theta,\delta)$ is given by [23]

$$\hat{U}(\theta,\delta)=\begin{pmatrix} \frac{1}{2}(1+\cos\theta) & -\frac{i}{\sqrt{2}}\sin\theta e^{-i\delta} & -\frac{1}{2}(1-\cos\theta)e^{-2i\delta} \\ -\frac{i}{\sqrt{2}}\sin\theta e^{i\delta} & \cos\theta & -\frac{i}{\sqrt{2}}\sin\theta e^{-i\delta} \\ -\frac{1}{2}(1-\cos\theta)e^{2i\delta} & -\frac{i}{\sqrt{2}}\sin\theta e^{i\delta} & \frac{1}{2}(1+\cos\theta) \end{pmatrix}. \tag{9}$$

Substituting $\mathbf{q}$ from Eq. (5), it may be found that there exist two values of $\theta$ such that for each of them the new vector $\mathbf{q}'$ consists of one circular and one linear component (instead of two circular). These two angles (with corresponding expansions in polarization components) are

$$\theta_1=\arccos(\tan\varepsilon):\quad q'_{+1}=0,$$

$$q'_0=-i\sqrt{\cos 2\varepsilon},\quad q'_{-1}=\sqrt{2}\sin\varepsilon, \tag{10a}$$

$$\theta_2=\pi-\arccos(\tan\varepsilon):\quad q'_{+1}=-\sqrt{2}\sin\varepsilon,$$

$$q'_0=-i\sqrt{\cos 2\varepsilon},\quad q'_{-1}=0. \tag{10b}$$

If the quantization axis is now directed along the new polarization vectors (hereafter referred to as the EDS axes), the selection rules become $\Delta m'=0,+1$ (or $\Delta m'=0,-1$). As a result, this transformation leads to the coupling scheme shown in Figs. 1(e) and 1(f) for $P$ and $Q$ transitions, respectively. In the former case, the existence of a noncoupled edge sublevel with the maximum projection of the angular momentum on the EDS axis ($m'=J$ or $m'=-J$) means that the dark state is formed by molecules which are oriented in this direction. Since there are two such directions ($\theta_{1,2}$), a *biaxial* orientation may be expected, as we have recently demostrated [21]. In the case of a $Q$ transition [Fig. 1(f)], a noncoupled sublevel does not exist and the rotational anisotropy is not as clear, although the presence of the $\Lambda$-type coupling manifests CPT in a new basis. Note, that the change of coordinate system does not ''generate'' uncoupled or $\Lambda$-coupled sublevels for the $R$ transition (not shown), explaining the absence of the dark states, which cannot depend on the choice of the quantization axis.

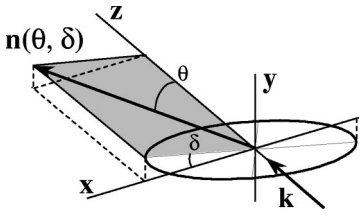


FIG. 3. Spherical coordinates $(\theta,\delta)$ of the new quantization axis. The wave vector of the exciting light $\mathbf{k}$ is collinear with the $\mathbf{z}$ axis, and the angle between the major axis of the polarization ellipse and the $\mathbf{x}$ axis is $\delta$.

### C. Angular momentum distribution

The angular momentum distribution may be calculated using the coherent states representation [4,24]. The angular momentum coherent state $|\Omega\rangle$ associated with the unit vector $n(\theta,\varphi)$ is defined by

$$|\Omega\rangle=\exp(-i\varphi\hat{J}_z)\exp(-i\theta\hat{J}_y)|JJ\rangle \tag{11}$$

and corresponds to the $|J,M=J\rangle$ state of the conventional basis rotated by an angle $\theta$ around the $\mathbf{y}$ axis and then by $\varphi$ around the $\mathbf{z}$ axis [same as vector $n(\theta,\delta)$ in Fig. 3 except that polar angle $\varphi$ is a free parameter not necessarily equal to the orientation angle $\delta$ of the polarization ellipse]. In the classical limit, for large $J$, the probability density function $\rho(\Omega)$ may be introduced as $\rho(\Omega)=\langle\Omega|\hat{\rho}|\Omega\rangle$, where $\hat{\rho}$ is the density matrix operator. In this limit, $\rho(\Omega)d\Omega$ represents the probability that the angular momentum $\mathbf{J}$ points inside the solid angle $d\Omega=\sin\theta d\theta d\varphi$ around the spatial direction $(\theta,\varphi)$. Thus $\rho(\Omega)$ has a meaning of a spatial distribution of the angular momentum. It may be obtained from the density matrix elements in the $|J,m\rangle$ basis as

$$\rho(\Omega)=\sum_{m,m'}\{A^J_m A^J_{m'}e^{i(m'-m)\varphi}[\cos(1/2\theta)]^{2J-m-m'} \times[\sin(1/2\theta)]^{2J+m+m'}\rho_{mm'}\}, \tag{12}$$

where

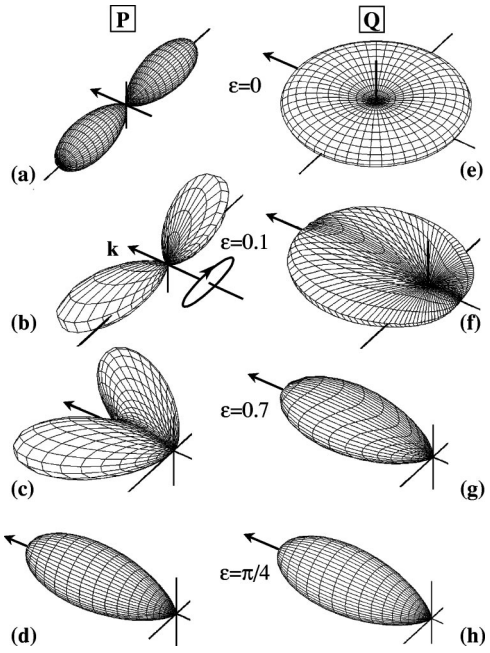


FIG. 4. The angular momentum distribution of the elliptical dark state created within $P$ (left column) and $Q$ (right column) transition for different ellipticities of the exciting light: (a),(e): $\varepsilon=0$, linear; (b),(f): $\varepsilon=0.1$; (c),(g): $\varepsilon=0.7$; (d),(h): $\varepsilon=\pi/4$, circular. The arrows point the direction of the light **k** vector, and the orientation of the polarization ellipse is shown in (b).

$$A_m^J=\sqrt{\left(\frac{2J!}{(J+m)!(J-m)!}\right)}.$$

An important conclusion is already derived from the simple analysis of Eq. (12): if no coherences are created ($\rho_{m,m'}=0$ for $m\neq m'$), as in the case of linear and circular polarization with a properly chosen quantization axis, a uniaxial distribution $\rho(\Omega)\equiv\rho(\theta)$ is obtained (see Fig. 4, the top and the bottom rows). For elliptical polarization, however, many $m$ sublevels are coupled by coherent field, and nonzero coherence terms must be considered in *any* coordinate system. The angular momentum distribution is therefore $(\theta,\varphi)$ dependent, and will not have a single symmetry axis.

The angular momentum distributions of a dark state created within the $P(10)$ and $Q(10)$ transitions are shown in Fig. 4 for linear, two different elliptical, and circular polarizations of the exciting light. The minor axis of the polarization ellipse is taken to coincide with the vertical axis (**y** axis). In all cases the long-time steady state is considered. In the $P$ case, $\rho(\Omega)$ in general has two spatial peaks which point along the two EDS axes defined by $\theta_{1,2}$ in Eq. (10). When the ellipticity parameter $\varepsilon$ changes from 0 (linear polarization) to $\pi/4$ (circular polarization), the distribution axes ''move'' in the plane defined by the wave vector **k** of the exciting light and the major axis of the polarization ellipse (**x**-**z** plane). Namely, for $\varepsilon=0$ the EDS axes are antiparallel, resulting in a standard longitudinal alignment depicted in Fig. 4(a). They twist towards the **k** vector (or rotate around **y**) as $\varepsilon$ increases [(b) and (c)], and finally merge to one orientation peak (d) for $\varepsilon=\pi/4$.

In contrast, in the $Q$ case, the distribution is not cyllindrically symmetric but rather flattened. At $\varepsilon=0$, a transverse pancakelike alignment is created [Fig. 4(e)], which then transforms to the elongated single-peak orientation ($\varepsilon\neq0$), and finally possesses an axial symmetry when $\varepsilon$ equals $\pi/4$ [plot (h)].

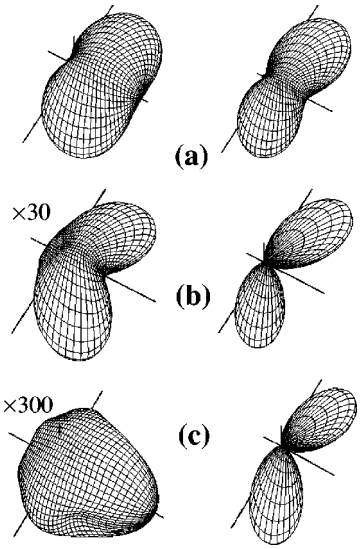


FIG. 5. The calculated dynamics of the distribution of angular momentum created within $J=20\rightarrow J=21$ (left column) and $J=20\rightarrow J=19$ (right column) transition by optical pumping with elliptically polarized light ($\varepsilon=0.4$). The interaction time is (a) $\tau$, (b) $5\tau$, (c) $8\tau$ ($\tau$ is the spontaneous lifetime of the excited state). Two axes of anisotropy (EDS axes) are clearly seen. The absence of the stationary state in the $\Delta J=1$ (left) case results in a severe population loss [depicted by the scaling factor in plots (b) and (c)], and the disappearance of the biaxial orientation at long interaction times.

To study time evolution of the distribution, the time-dependent density matrix elements were found numerically from Eq. (3). To simulate realistic situation, the initial conditions were of equally populated sublevels with no cross coherences between them, and the results were averaged over random initial phases of the ground state wave function amplitudes $b_m$. In Fig. 5 the calculated time evolution of the angular momentum distribution $\rho(\theta,\varphi)$ is shown for two types of transitions, $\Delta J=\pm1$. If the interaction time is shorter than the optical pumping time $t_{\mathrm{op}}$ [plot (a)], the spatial anisotropy is not very pronounced. In Fig. 5(b) the distribution at $t=5t_{\mathrm{op}}$ is depicted, showing a similar biaxial geometry for both cases, although the enlarged scale for $\Delta J=1$ transition indicates a significant population loss of the nonstationary state. After a longer interaction time [plot (c)], the biaxial distribution $\rho(\theta,\varphi)$ in the $P$ case remains stable, as the system approaches the stationary noncoupled dark state (EDS), while the nonstationary state is almost empty. From the above, it is clear that $P$ and $Q$ transitions, which support coherent population trapping, are the best candidates for studying effects of optical orientation of the angular momentum in open systems.

## III. CLASSICAL APPROACH

In the classical approach the molecule is treated as a rigid rotator, and any possible correlations between the magnetic sublevels are neglected. In the CPT case, this approximation is not strictly valid due to the laser-induced long-range coherences between many $m$ sublevels. In this sense, the ellip-

tical dark state is an example of a nonclassical state of a molecular rotor, even in the case of a large value of the angular momentum. The question arises, however, whether the classical picture is even approximately valid for high $J$'s, and what are the limits of its applicability. This problem was first addressed by Drullinger and Zare in Ref. [5], who studied the degree of polarization of laser-induced fluorescence in optical pumping of molecules. The comparison between the classical and quantum treatements of the low intensity linearly polarized excitation, calculated in the rate equations approximation, showed that already for $J \geqslant 5$ the results are almost the same. At high intensities, however, serious disagreements between the classical predictions and experimental observations were found. The experimentally measured degree of polarization was much higher than its classically calculated value.

The problem of the equivalence of the classical and quantum approaches was at the focus of many theoretical and experimental works (for a review, see Ref. [25], and references therein). As was originally shown by Ducloy [2,4] and later investigated in depth by Auzin'sh and Ferber [7,26], the exact (for any $J$) equations for the density matrix $\rho(\Omega,\Omega')$ in the coherent states representation may be expanded over the irreducible tensorial set of polarization moments $\rho_Q^k$ (''$kQ$ representation''). Here the $Q$ number corresponds to the order (in $\Delta m$) of the laser-induced coherence. Since the diagonal elements of the density matrix represent the angular momentum distribution, this distribution may, in principle, be obtained by integrating the equations of motion of the polarization moments followed by further reconstruction of $\rho$. For high $J$'s, however, the number of equations is too large ($0 \leqslant k \leqslant J$, $|Q| \leqslant k$), and this method of finding $\rho$ becomes practically impossible. On the other hand, in the classical limit, the off-diagonal matrix elements $\rho(\Omega,\Omega')$ ($\Omega \neq \Omega'$) may be neglected, since the absorption (emission) of one photon with spin 1 by a high-$J$ rotor cannot change the direction of **J** substantially. In this case, the classical Bloch equations may be written and solved analytically. In what follows, we apply the classical approach to the case of elliptically polarized light, and compare the classical and quantum predictions.

### A. Classical equations for the density matrix

The classical equations for the diagonal elements of the density matrix were obtained by Ducloy [3], and later generalized by Nasyrov and Shalagin [27] for a two-level system with laser-induced coherences. In the rotating wave approximation and for the case of spontaneous emission as the only relaxation mechanism, these equations are

$$\begin{aligned}
\dot{\rho}_{aa}(\Omega) &= 2\,\mathrm{Re}[iV_{ab}^*(\Omega)\rho_{ab}(\Omega)] - 2\gamma\rho_{aa}(\Omega), \\
\dot{\rho}_{bb}(\Omega) &= -2\,\mathrm{Re}[iV_{ab}^*(\Omega)\rho_{ab}(\Omega)], \\
\dot{\rho}_{ab}(\Omega) &= iV_{ab}(\Omega)[\rho_{bb}(\Omega) - \rho_{ab}(\Omega)] - \gamma\rho_{ab}(\Omega).
\end{aligned} \tag{13}$$

As can be seen, Eqs. (13) have a structure which is well known for a two-level system, except for the parametric dependence of all matrix elements on an external parameter $\Omega$. This parameter determines the two spherical angles ($0 \leqslant \theta \leqslant \pi, -\pi \leqslant \varphi \leqslant \pi$) that characterize the direction of the classical angular momentum (Fig. 3). The indexes $a$ and $b$ correspond to the excited and ground states, respectively, and $2\gamma$ is the rate of spontaneous emission decay from the excited level out of the system (for simplicity we will consider a totally open system, i.e., the probability of returning to the same ground state is zero). Note, that we keep one-photon coherences, and neglect all higher order ones.

The classical interaction Hamiltonian may be written as a product of the dynamic part $W$, and the angular part $V(\theta,\varphi) = \mathbf{qd}^*$, determined by the Hermitian product of the light polarization vector **q** and the unit vector **d**. Then for $V_{ab}(\Omega)$ we have

$$V_{ab}(\Omega) = W \times V(\theta,\varphi) = W \times \sum_{Q=-1}^{1} (-1)^Q \mathbf{q}_Q D_{\Delta Q}^{1*}(0,\theta,\phi). \tag{14}$$

Here $\mathbf{q}_Q$ are the cyclic components of the polarization vector, $D_{\Delta Q}^1(0,\theta,\phi)$ is the Wigner $D$ matrix, and the type of transition is defined by $\Delta = J_a - J_b$. Using an explicit form of $D_{\Delta Q}^1(0,\theta,\phi)$:

| $\Delta \backslash Q$ | 1 | 0 | −1 |
|---|---|---|---|
| 1 | $\frac{1}{2}(1+\cos\theta)e^{-i\varphi}$ | $\frac{1}{\sqrt{2}}\sin\theta$ | $\frac{1}{2}(1-\cos\theta)e^{i\varphi}$ |
| 0 | $\frac{1}{\sqrt{2}}\sin\theta e^{-i\varphi}$ | $\cos\theta$ | $-\frac{1}{\sqrt{2}}\sin\theta e^{i\varphi}$ |
| −1 | $\frac{1}{2}(1-\cos\theta)e^{-i\varphi}$ | $\frac{1}{\sqrt{2}}\sin\theta$ | $\frac{1}{2}(1+\cos\theta)e^{i\varphi}$ |

one obtains for $P$ and $R$ transitions ($\Delta = -1$ and $\Delta = +1$, respectively)

$$\begin{aligned}
|V(\theta,\varphi)| = \tfrac{1}{2}[1 + \cos^2\theta + 2\Delta\cos\theta\sin 2\varepsilon \\
- \sin^2\theta\cos 2\varepsilon\cos 2(\varphi - \delta)]^{1/2},
\end{aligned} \tag{15}$$

where the polarization parameters $\varepsilon$ and $\delta$ were defined in Eq. (5). For $Q$ transitions ($\Delta = 0$) we find

$$|V(\theta,\varphi)| = \frac{\sin\theta}{\sqrt{2}}[1 + \cos 2\varepsilon\cos 2(\varphi - \delta)]. \tag{16}$$

### B. Time-dependent solution

In Ref. [27], the steady-state solution of Eqs. (13) was found. To prevent the emptying out of an open system, the authors introduced an isotropic flux of molecules into the ground and excited states. However, in many cases this model is not adequate. For example, when molecules pass through a laser beam, the population or the angular momentum distribution *at the exit* of the interaction zone is determined by the time of flight across the beam, and cannot be found as a steady-state solution. Thus, the full time-dependent solution of Eqs. (13) is needed. If the excited state was initially empty, $\rho_{bb}(\Omega) = 1$, $\rho_{aa}(\Omega) = \rho_{ab}(\Omega) = 0$, the solution for the ground-state population is given by

$$\rho_{bb}(\theta,\varphi)=\frac{1}{4\Gamma^2}[(\gamma-\Gamma)^2e^{-(\gamma+\Gamma)t}+(\gamma+\Gamma)^2e^{-(\gamma-\Gamma)t} -8W^2|V(\theta,\varphi)|^2e^{-\gamma t}], \quad (17)$$

$$\Gamma=\sqrt{\gamma^2-4W^2|V(\theta,\varphi)|^2}.$$

Although the coherent population trapping is lost in this picture (due to the omission of coherences), the angular momentum distribution of the ground-state molecules $\rho_{bb}(\Omega)$ strongly depends on the spherical angles $(\theta,\varphi)$. In fact, the ground state is not at all depleted in the directions of zero interaction strength $|V(\theta,\varphi)|=0$, if such directions exist. For any other direction, the stationary solution is zero due to the spontaneous decay out of the system.

In terms of the interaction strength, one may consider strong and weak excitation, as determined by the saturation parameter $\varkappa=W^2/\gamma^2$. For weak excitation ($\varkappa\ll1$), the approximate solution is given by

$$\rho_{bb}(\theta,\varphi)\simeq e^{-2\gamma\varkappa|V(\theta,\varphi)|^2t}, \quad (18)$$

which describes the anisotropic relaxation of the ground state at the rate $\gamma_{\rm op}=2\gamma\varkappa|V(\theta,\varphi)|^2$. This process results in a $(\theta,\varphi)$-dependent angular momentum distribution.

For strong excitation ($\varkappa\gg1$), two situations may be distinguished

$$\varkappa|V(\theta,\varphi)|^2\ll1, \quad (19a)$$

$$\varkappa|V(\theta,\varphi)|^2\gg1. \quad (19b)$$

The first condition determines the directions of a ''slow depletion,'' when Eq. (18) holds again. Along the directions determined by Eq. (19b), the population oscillates at the well known Rabi frequency and decays to zero with an isotropic optical pumping rate $\gamma_{\rm op}=\gamma$, as given by

$$\rho_{bb}(\theta,\varphi)\simeq e^{-\gamma t}\{\cos[W|V(\theta,\varphi)|t]\}^2. \quad (20)$$

The important conclusion of this analysis may be summarized as follows: for above-saturation light intensities the orientational features of $\rho_{bb}(\theta,\varphi)$ are mostly determined by the saturation parameter, whereas in the weak-excitation regime the duration of interaction plays a key role.

## IV. VALIDITY OF THE CLASSICAL APPROXIMATION

### A. Weak-field limit

Equations (17) and (15) yield the classical distribution in the case of a $P$ transition, and this distribution is depicted in Fig. 6(a). The two narrow spatial peaks (''whiskers'') of this distribution correspond to the zeros of the angular part of the classical interaction Hamiltonian ($|V(\theta,\varphi)|=0$):

$$\cos\theta_{1,2}=\tan\varepsilon, \quad \varphi=\delta. \quad (21)$$

One can see that these two spatial directions $(\theta_{1,2},\varphi)$ coincide exactly with the two EDS axes determined by Eqs. (10a),(10b). It is now clear (and not surprising) that for a $P$ transition, which supports coherent population trapping, $\rho_{bb}(\theta,\varphi)$ in the directions of the EDS axes represent the classical analog of the population of a noncoupled $m$ sublevel. Therefore, the limits of applicability of the classical treatment may already be formulated: the width of the spatial ''whiskers'' of the angular momentum distribution cannot be smaller than the quantum uncertainty, which could be estimated as

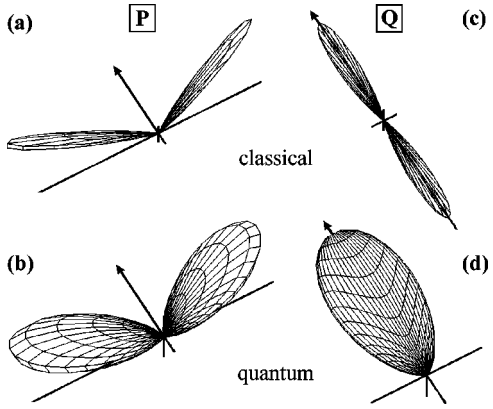


FIG. 6. The angular momentum distribution for low intensity $\varkappa=0.1$ and interaction time much longer than the characteristic time of optical pumping $t=10t_{\rm cl}$. Left column: $P$ transition, right column: $Q$ transition. Upper row: classical approximation; lower row: exact quantum solution. The distribution ''whiskers'' of the classical picture are much narrower than the quantum uncertainty limit.

$$(\Delta\theta)^2\geqslant\langle J_x^2+J_y^2\rangle/J^2\sim1/J. \quad (22)$$

In the quantum picture, the elliptical dark state is completely formed if the interaction time is longer than the time of optical pumping, which for a weak excitation ($\varkappa\ll1$) is given by $t_{\rm op}=(\varkappa\gamma)^{-1}$ [Eq. (6)]. In this limit, from Eq. (18) and from the expansion of Eq. (15) around the zeros of $|V(\theta,\varphi)|$, one obtains

$$(\Delta\theta)^2\ll(\gamma t\varkappa\cos2\varepsilon)^{-1} \quad \text{for} \quad \cos2\varepsilon>\sqrt{1/\gamma t\varkappa}, \quad (23a)$$

$$(\Delta\theta)^2\ll(\gamma t\varkappa)^{-1/2} \quad \text{for} \quad \cos2\varepsilon<\sqrt{1/\gamma t\varkappa}, \quad (23b)$$

where (b) defines an almost circular polarization ($\varepsilon\simeq\pm\pi/4$). For elliptical polarization, Eq. (23a) and Eq. (22) provide the validity condition of the classical approximation

$$t<t_{\rm cl}\equiv J(\gamma\varkappa)^{-1}. \quad (24)$$

This result is illustrated in Fig. 6, where the classical (top) and the quantum (bottom) angular momentum distributions are presented for $t>t_{\rm cl}$. (Hereafter, the ellipticity parameter used in our numerical analysis is 0.1 for $P$ transition, and 0.7 for $Q$ transition.) If the duration of the interaction is longer than $t_{cl}$, the classical distribution is narrower than the ''quantum-uncertainty limit'' and the classical treatment is not valid [compare plots (a) and (b)].

The same analysis may be applied for the $Q$ transition [Figs. 6(c) and 6(d)]. Note that the classical distribution is not only narrower than the exact result of the quantum calculations, but also possesses an incorrect symmetry. It has two symmetrical maxima specified by the directions of the zero interaction strength, which in the $Q$ case are

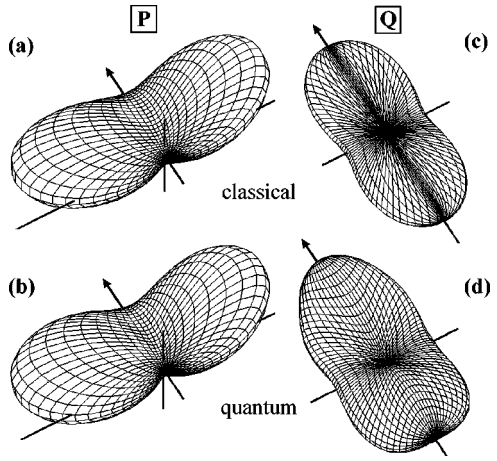


FIG. 7. The angular momentum distribution for short interaction time $t=0.5t_{\rm cl}$ and low intensity $\varkappa=0.1$. Left column: $P$ transition, right column: $Q$ transition. Upper row: classical approximation, lower row: exact quantum solution. The classical pictures are generally similar to their quantum counterparts.

$$\theta_{1,2}=0,\pi, \tag{25}$$

whereas only one of these angles is supported quantum mechanically. Indeed, as was discussed in Sec. II A, the two ground-state edge $m$ sublevels of the $Q$ transition ($m=J$ and $m=-J$) may never be equally populated under elliptically polarized excitation (one of them may, in principle, be empty). This breaks the symmetry of the angular momentum distribution, and again limits the validity of the classical picture.

For short interaction times, $t<t_{\rm cl}$, the spatial peaks of the classical picture are wider than the ''quantum uncertainty limit.'' Thus, the classical approximation is valid in both the $P$ and $Q$ cases as may be clearly seen in Fig. 7, where the quantum-to-classical correspondence is very good.

### B. Strong-field limit

As was derived in Sec. III B, the spatial anisotropy of $\rho_{bb}(\theta,\varphi)$ in the two cases of ''above saturation'' limit [$\varkappa\gg1$, Eq. (19)] stems from the existence of directions of slow and fast depletion, determined by the parameter $\varkappa|V(\theta,\varphi)|^2$. This anisotropy of the angular momentum distribution will show up already after the time $t\sim\gamma^{-1}$, where $\gamma$ specifies the fast depletion rate given by Eq. (20). On the other hand, the spatial width of the distribution is defined by the spherical angles $(\theta,\varphi)$ of the slow depletion directions determined by condition $\varkappa|V(\theta,\varphi)|^2\ll1$ [Eq. (19a)], and the expansion of Eq. (15) for $P$ and Eq. (16) for $Q$:

$$(\Delta\theta)^2\ll(\varkappa\cos2\varepsilon)^{-1} \quad \text{for} \quad \cos2\varepsilon>\sqrt{1/\varkappa}, \tag{26a}$$

$$(\Delta\theta)^2\ll(\varkappa)^{-1/2} \quad \text{for} \quad \cos2\varepsilon<\sqrt{1/\varkappa}. \tag{26b}$$

Combining Eq. (26a) (corresponding to the elliptical polarization) with the quantum uncertainty limit [Eq. (22)], we obtain the same identical result for both the $P$ and $Q$ transitions under the strong field excitation. The classical approximation is generally valid as long as the saturation parameter is not too large and satisfies the condition

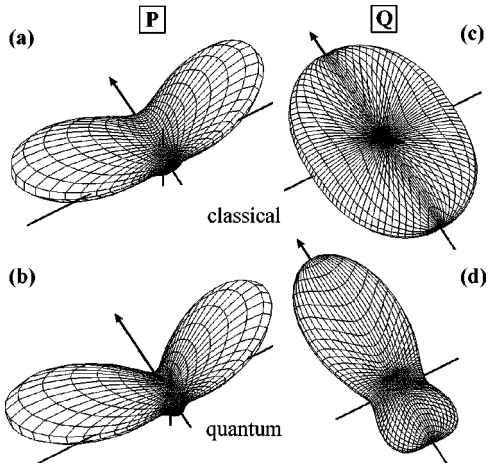


FIG. 8. The angular momentum distribution for short interaction time $t=2\gamma^{-1}$ and the ''above-saturation'' but not too high light intensity $\varkappa=0.5\varkappa_{\rm cl}$. Left column: $P$ transition, right column: $Q$ transition. Upper row: classical approximation, lower row: exact quantum solution. The quantum-to-classical analogy holds for the $P$ case, but fails in the case of $Q$ transition.

$$\varkappa<\varkappa_{\rm cl}\equiv J. \tag{27}$$

At the not too high intensities given by Eq. (27), the classical distribution in the case of a $P$ transition is very similar to the quantum one [Figs. 8(a) and 8(b)]. In contrast, for $Q$ transitions the comparison of the plots (c) and (d) shows that the classical approximation fails already at $\varkappa\lesssim\varkappa_{\rm cl}$. Even though the width of the $J$ distribution is not limited by the quantum uncertainty, the symmetry of $\rho_{bb}(\theta,\varphi)$ differs from the exact quantum solution, where only one ''whisker'' builds up in time. As was discussed before, the disagreement originates from one ''wrong'' zero of the classical interaction Hamiltonian [Eq. (16)], resulting in a nondirectional (alignmentlike) anisotropy instead of a directional (orientationlike) one. Finally, the quantum uncertainty limit is reached in the regime of $\varkappa>\varkappa_{\rm cl}$ as may be seen by comparing the plots (a) with (b), and (c) with (d) in Fig. 9, where the classical approximation fails in both $P$ and $Q$ cases.

To summarize this comparison, one may draw the following conclusion: for a $P(J)$ ($J\gg1$) transition, the classical approximation may be used for short interaction times $t<t_{\rm cl}$, and moderate light intensities, $1<\varkappa<J$. For $Q$ transitions, however, only the short time limit, $t<t_{cl}$, allows the use of the classical picture, and any deviation from the weak field case ($\varkappa\ll1$) will result in an incorrect symmetry of the angular momentum distribution. The different behavior of the two types of transition stems from their different internal structure, where one of the $\Lambda$ coupling chain ($P$) is replaced by the $V$ type of coupling ($Q$). During the interaction with the $Q$ transition, the sublevels of the $V$ configuration are completely depopulated. This quantum-mechanical aspect of the interaction is ignored by the classical description.

## V. EXPERIMENTAL OBSERVATION

### A. CPT-Hanle effect

As was demonstrated above, the best manifestation of the biaxial orientation may be obtained with the stationary ellip-

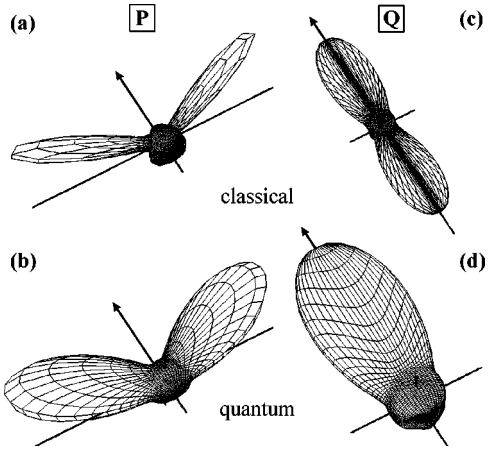


FIG. 9. The angular momentum distribution for short interaction time $t=2\gamma^{-1}$ and very high light intensity $\varkappa=5\varkappa_{\rm cl}$. Left column: *P* transition, right column: *Q* transition. Upper row: classical approximation, lower row: exact quantum solution. The EDS is almost formed, and the classical picture fails to describe the *J* distribution in either *P* or *Q* cases.

tical dark states. The biaxial symmetry of the angular momentum distribution of the EDS created within the *P* transition may be observed by means of CPT-Hanle configuration, as we have recently reported in Ref. [21]. The standard Hanle effect [28,29] is manifested as depolarization of the laser-induced fluorescence in an external magnetic field. In ''classical'' language, the phenomenon stems from the Larmor precession of the molecular magnetic dipole moment (and therefore, of the entire angular momentum distribution) around the applied magnetic field **H** with angular frequency $\omega_J=g_J\mu_0H/\hbar$. Here $g_J$ is the Landé factor and $\mu_0$ is the Bohr magneton. Since the polarization of re-emitted photons is sensitive to the direction of **J**, the degree of polarization of the fluorescence, averaged over the precession time, changes with the magnetic field [25].

In the CPT-Hanle configuration, the *total fluorescence* signal is measured as a function of the magnetic field strength. In the quantum picture, an external magnetic field lifts the degeneracy of the magnetic sublevels and destroys the coherent population trapping by violating the condition of the destructive interference between the interaction pathways. The dark state is not stationary at $H\neq 0$, and therefore all molecules are excited and contribute to the fluorescence signal, until the ground state is empty after the characteristic time $t_{\rm op}$ [Eq. (6)]. At zero field, however, part of the population is trapped in the dark state and does not participate in the interaction, thus minimizing the number of re-emitted photons. Effectively, an applied magnetic field affects the number of interacting particles, and the total fluorescence is minimal at $H=0$—the CPT-Hanle resonance [30,31]. Note that even a nonzero field directed along the EDS axis will not completely ruin the CPT due to the existence of a noncoupled *m* sublevel [see Fig. 1(c)] which will not be mixed with other sublevels. Thus, the resonance may be assigned not to a zero magnetic field but rather to a zero component along a certain direction.

As in the case of standard Hanle effect, the CPT Hanle resonances may be explained classically. Namely, the Larmor precession of the total angular momentum around the applied magnetic field leads to the mismatch between the light polarization and the angular momentum distribution, thus destroying the dark state. The precession competes with the laser-induced orientation unless the magnetic field and orientation axes are collinear. Therefore, when one scans the direction of a constant magnetic field in the plane of the two EDS ''whiskers,'' the biaxial geometry will result in two Hanle resonances—one for each EDS axis.

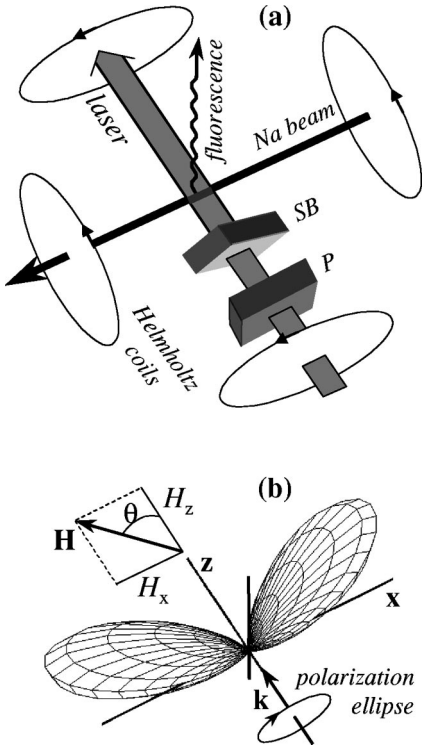


FIG. 10. (a) The geometrical arrangement of the laser beam, the sodium atomic beam, and the direction of observation. Polarizer *P* and Soleil-Babinet compensator SB are used to define the polarization ellipticity of the exciting light. (b) Mutual orientation of the polarization ellipse, the EDS angular momentum distribution, and the applied magnetic field **H** which is scanned in the plane of the EDS axes (**x**-**z** plane).

### B. Results

To verify this model experimentally, we measure the total fluorescence signal at right angle to the mutually perpendicular collimated collisionless atomic beam of sodium and a laser beam, resonant with the $D_1$ $F=2\rightarrow F=1$ hyperfine transition. The experimental geometry is depicted in Fig. 10(a). The ''above saturation'' laser intensity (40 mW/cm$^2$) and long interaction time ($\sim$400 excited state lifetimes, $t\gg t_{\rm op}$) assure that all atoms entering the laser beam are pumped either into the dark state ($F=2$ ground manifold), or to the nonresonant $F=1$ ground level. The time of interaction, regulated by the diameter of the laser beam (usually, about 5 mm), and the light intensity are adjusted for maximum contrast of the CPT-Hanle signal. The light ellipticity is accurately set by a Soleil-Babinet compensator [*SB* in Fig. 10(a)]. The optical axis of the SB is fixed at 45° with respect to the input polarizer *P*, which therefore defines the major axis of the polarization ellipse to be parallel to the atomic beam. Three pairs of Helmholz coils are used to scan the

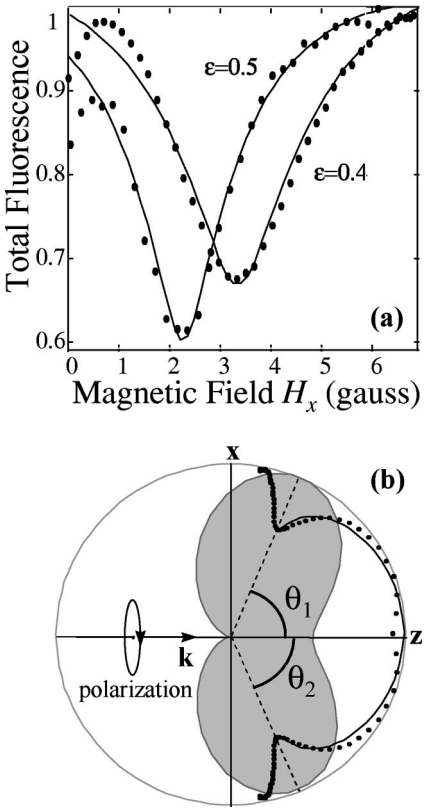


FIG. 11. (a) Measured (dots) and calculated (line) total fluorescence intensity as a function of the $x$ component of the magnetic field ($H_z = 1.5$ G) for two different elliptical polarizations. (b) The measured fluorescence intensity (dots) in polar coordinates as a function of the magnetic field orientation angle $\theta$. Shaded region represents the calculated $J$ distribution in the **x-z** plane. The solid line is the result of the numerical calculation.

direction of the external magnetic field [only two of them are shown in the figure). The mutual orientation of the polarization ellipse, the external magnetic field, and the laser-induced biaxial orientation of the atomic angular momentum are shown in Fig. 10(b)].

The measured fluorescence intensity is given in Fig. 11(a) as a function of the magnetic field component in the **x** direction, while the **y** component is zero, and the **z** component is kept fixed. In Fig. 11(b) the data is shown in polar coordinates as a function of the magnetic field orientation angle $\theta$. In this figure, the calculated angular momentum distribution in the **x-z** plane is plotted in gray. The correspondence between the Hanle dips and the EDS axes is clearly visible. For a given ellipticity $\varepsilon$, the orientation angles $\theta_{1,2}$ at Hanle resonance are found to be in a good agreement with the theoretical prediction $\cos\theta_{1,2} = \pm\tan\varepsilon$.

It should be mentioned that the magnetic field was weaker than 8 G, meaning that the Zeeman splitting (2.8 MHz/G for the $|m| = 2$ sublevels) is less than the width of the power broadened transition ($>25$ MHz), and the interaction may be considered resonant with all the magnetic sublevels. For a larger magnetic field ($>100$ G, recently used in Ref. [32]), the splitting will be larger than the transition linewidth and the number of the interacting levels will be reduced to three, as in a ''classical'' $\Lambda$ system. The CPT Hanle resonances observed in our experiment must not be confused with the standard Hanle dips at nonzero field, corresponding to the large order laser-induced coherences even whithout the CPT [3].

### C. Comparison with numerical calculations

In order to calculate the fluorescence signal numerically, the full Bloch equations for the density matrix must be calculated. However, in the case of EDS in an external magnetic field, a simplified ''rate equations'' approximation may be justified if the equations are calculated in a rotated basis where the quantization axis is taken to be directed along either one of the two EDS axes. In this case, the existence of a noncoupled sublevel ($m = 2$, in our case) with no cross coherences ''prevents'' its population from being excited. In other words, a choice of the basis in accordance with the light ellipticity ''emulates'' the CPT by calculating the incoherent optical pumping to a noncoupled state. In a zero magnetic field, this approximation is only partly valid, since half of the atoms are still trapped in the multi-$\Lambda$ system, which is also present in the new chosen basis [see Fig. 1(e)]. However, if the rate of magnetic dephasing (1.4 MHz/G) is larger than the transit decay rate of the ground state ($\ll 1$ MHz in our experiment), the coherences between the sublevels with $-2 < m < +1$ average out to zero and can safely be neglected. Thus, this rate equation approach is expected to be valid for $H > 1$ G, which is the case in our experiments, and, while being only an approximation, provides an intuitive explanation for the behavior in external magnetic fields. In the calculation, we introduced the effect of the magnetic field as an isotropic rate of the ground state sublevels population redistribution towards uniform (as given by the time averaging over many precession cycles). The decay rate was taken to be equal to the Larmor frequency corresponding to the perpendicular (to the EDS axis) component of the magnetic field. The results of numerical calculations of the light-induced fluorescence intensity in the presence of an external magnetic field are shown by a thin line in Fig. 11(a). Indeed, in the region of relatively strong magnetic fields the fit is very good. Finally, it should be noted that this approximation cannot be applied in the case of $Q$ transition due to the absence of the noncoupled states in any chosen coordinate system.

## VI. CONCLUSIONS

The polarization ellipticity of the exciting light provides an additional degree of freedom in controlling the angular momentum distribution of atoms and molecules. As we have shown here, very narrow spatial distributions limited by the quantum uncertainty may be achieved on $P$ and $Q$ transitions, which support coherent population trapping. Moreover, in the case of a $P$ transition, a biaxial orientation (where the angle between the two preferential directions of $J$ is determined by the light polarization) may be created. The ensemble of particles is optically pumped into the elliptical dark state—a coherent superposition of the ground-state magnetic sublevels. The laser-induced coherences between the ground-state magnetic sublevels define the rotational anisotropy of the EDS, which therefore cannot be described as a classical object even for a large angular momentum. In the limit of long interaction times, much longer than the charac-

teristic time for optical pumping, and high laser intensities, when the saturation parameter is larger than $J$, the quantum nature of CPT restricts the angular dimensions of the orientation peaks. The classical approximation, where a molecule is considered as a classical rotor, may be successfully used in the limits of moderate light intensity and short interaction time. For $Q$ type transitions at the ''above saturation'' regime of excitation, any ellipticity of the exciting light will result in orientationlike distribution, which cannot be predicted by classical means. In contrast, the biaxial orientation induced within the $P$ type transitions is well described classically unless the quantum uncertainty limit is approached.

The preparation of molecular elliptical dark states may prove useful for the creation of arbitrary orientation of angular momentum, which does not coincide either with the light wave vector or with the vector of linear polarization. Indeed, once the magnetic field direction is parallel to one of the EDS axes, only one spatial peak of the angular momentum distribution ''survives'' the Larmor precession. The atoms or molecules belonging to this peak are therefore well oriented along the chosen direction, dictated by the polarization ellipticity. Thus, in order to create an arbitrary orientation, one needs to select the ellipticity according to the desired orientation angle and to apply a weak magnetic field along this direction. This method of producing arbitrarily oriented ensembles of neutral atoms or molecules, so often required in various collision experiments, is different from the earlier technique of stimulated Raman adiabatic passage in multilevel systems [33–35]. Orientation by elliptically polarized light is less sensitive to the adiabaticity conditions and to the precise tuning of the two-photon transition, and may be achieved even with incoherent source, as we have demonstrated [21]. Note also that our method for the creation of an arbitrary orientation by coherent population trapping in a magnetic field is more powerful than alignment-to-orientation transformation by linearly polarized light in a weak magnetic field [36,37]. In the latter case, the resultant orientation is always collinear with the light propagation axis.

Finally, the new features of the elliptical dark states may be utilized for the magnetometric measurement of *arbitrarily* directed weak fields, so far not possible in a standard Hanle configuration where constant light polarization determines the magnetic field direction [38]. By scanning the light ellipticity $\varepsilon$ and the polarization ellipse orientation $\varphi$, the two spherical angles [or two spherical coordinates $\theta_{1,2}(\varepsilon)$ and $\varphi$] of the magnetic field could be measured when the Hanle dip is observed. The biaxial distribution of the EDS angular momentum will give incomplete information about the magnetic field orientation, since the two EDS axes give rise to the same Hanle resonance. Nevertheless, the two directions may be distinguished via the analysis of the degree of circular polarization of the laser-induced fluorescence [39]. Experiments are under way to utilize this possibility.

## ACKNOWLEDGMENTS

We wish to thank I. Sh. Averbukh, M. Ben-Chorin, and R. Ferber for useful discussions. This work was supported by grants from the Israel Science Foundation and the Minerva Foundation.

[1] A. Kastler, J. Phys. Radium **11**, 255 (1950).
[2] M. Ducloy, Phys. Rev. A **8**, 1844 (1973).
[3] M. Ducloy, Phys. Rev. A **9**, 1319 (1974).
[4] M. Ducloy, J. Phys. B **9**, 357 (1976).
[5] R. E. Drullinger and R. N. Zare, J. Chem. Phys. **51**, 5532 (1969).
[6] R. Altkorn, R. N. Zare, and C. H. Greene, Mol. Phys. **55**, 1 (1984).
[7] M. P. Auzin'sh and R. S. Ferber, Opt. Spektrosk. **68**, 256 (1990).
[8] U. Hefter *et al.*, J. Chem. Phys. **85**, 286 (1986).
[9] W. V. Davis, A. L. Gaeta, and R. W. Boyd, Opt. Lett. **17**, 1304 (1992).
[10] A. V. Bezverbnyj, V. S. Smirnov, and A. M. Tumaikin, Zh. Eksp. Teor. Fiz. **105**, 62 (1994) [J. Exp. Theor. Phys. **78**, 33 (1994)].
[11] A. Gahl *et al.*, Phys. Rev. A **50**, R917 (1994).
[12] R. Holzner *et al.*, Phys. Rev. Lett. **78**, 3451 (1997).
[13] J. R. Morris and B. W. Shore, Phys. Rev. A **27**, 906 (1983).
[14] G. Nienhuis, Opt. Commun. **59**, 353 (1986).
[15] V. Milner and Y. Prior, Phys. Rev. Lett. **80**, 940 (1998).
[16] V. S. Smirnov, A. M. Tumaikin, and V. I. Yudin, Sov. Phys. JETP **69**, 913 (1989).
[17] I. I. Sobelman, *Atomic Spectra and Radiative Transitions*, 2nd ed. (Springer-Verlag, Berlin, 1992).
[18] V. Milner, B. M. Chernobrod, and Y. Prior, Europhys. Lett. **34**, 557 (1996).
[19] E. Arimondo and G. Orriols, Lett. Nuovo Cimento **17**, 333 (1976).
[20] H. R. Gray, R. M. Whitley, and C. R. Stroud, Opt. Lett. **3**, 218 (1978).
[21] V. Milner and Y. Prior, Phys. Rev. A **59**, R1738 (1999).
[22] A. M. Tumaikin and V. I. Yudin, Sov. Phys. JETP **71**, 43 (1990).
[23] D. A. Varshalovich, A. N. Moskalev, and V. K. Hersonskij, *Quantum Theory of Angular Momentum* (Nauka, Leningrad, 1975).
[24] F. T. Arecchi, E. Courtens, R. Gilmore, and H. Thomas, Phys. Rev. A **6**, 2211 (1972).
[25] M. P. Auzinsh and R. S. Ferber, *Optical Polarization of Molecules* (Cambridge University Press, Cambridge, 1995).
[26] M. P. Auzin'sh and R. S. Ferber, Phys. Rev. A **43**, 2374 (1991).
[27] K. A. Nasyrov and A. M. Shalagin, Sov. Phys. JETP **54**, 877 (1981).
[28] W. Hanle, Z. Phys. **30**, 93 (1924).
[29] G. Breit, Rev. Mod. Phys. **5**, 91 (1933).
[30] J. L. Picque, J. Phys. B **11**, L59 (1978).
[31] F. Renzoni, W. Maichen, L. Windholz, and E. Arimondo, Phys. Rev. A **55**, 3710 (1997).

[32] R. Holler, F. Renzoni, L. Windholz, and J. H. Xu, J. Opt. Soc. Am. B **14**, 2221 (1997).
[33] R. Dopheide and H. Zacharias, J. Chem. Phys. **99**, 4864 (1993).
[34] B. W. Shore, J. Martin, M. P. Fewell, and K. Bergmann, Phys. Rev. A **52**, 566 (1995).
[35] J. Martin, B. W. Shore, and K. Bergmann, Phys. Rev. A **54**, 1556 (1996).
[36] M. P. Auzin'sh, Opt. Spectrosc. **68**, 695 (1990).
[37] Y. Nafcha, D. Albeck, and M. Rosenbluh, Phys. Rev. Lett. **67**, 2279 (1991).
[38] C. Cohen-Tannoudji, Phys. Scr. **T70**, 79 (1997).
[39] V. Milner, Ph.D. thesis, The Weizmann Institute of Science, 1998 (unpublished).